Supporting information

SI Results

Histone H3 binding affinities of the PHD finger and TTD. We measured the binding affinity of the histone H3 tail for the isolated PHD finger (residues 299-366) and isolated TTD (residues 123-285), and examined the effects of modifications on the histone H3 tail by using ITC. Our ITC data showed that the PHD finger selectively bound to unmodified histone H3 tail with high affinity (K_d = 1.73 μM). Tri-methylation of K9 in histone H3 caused no significant effect on binding (K_d = 1.47 μM), whereas the tri-methylation of K4 slightly reduced binding to the PHD finger (K_d = 4.50 μM). In contrast, asymmetric dimethylation of R2 (R2me2a) largely impaired binding (K_d = 12.70 μM) (Table S2 and Fig. S1). In addition, acetylation of the N-terminal amino group of histone H3 and phosphorylation of T3 almost completely abolished binding to the PHD finger (Table S2 and Fig. S1).

TTD bound more tightly to histone H3 tail containing K9me3 and showed no binding to histone H3 with a non-methylated K9 residue (Table S2 and Fig. S2). The methylated H3-K9 residue seems to be discriminated from other methylated lysine residues in histone tails by TTD alone, as the domain exhibited no detectable affinity for either a histone H3 tail containing K27me3 or a histone H4 tail containing K20me3 (Table S1 and Fig. S2). Collectively, the binding data indicate that the PHD finger and TTD of UHRF1 act as ‘readers’ of the histone modifications H3-R2me0 and H3-K9me3, respectively.

Structure of a complex formed between the isolated PHD finger and the histone H3 tail. We determined the crystal structure of a complex formed between the isolated PHD finger (residues 299-366) and the unmodified histone H3 tail (residues 1-10) at 1.4 Å resolution (Table S1 and Fig. S5*A*). The first nine residues of histone H3 were identified by the |*F*o|-|*F*c| omitted difference Fourier map (Fig. S5*A*). in the structure, the PHD finger is folded around three zinc atoms (Fig. S5*A*). The C-terminal region, containing a conserved Cys4-His-Cys3 motif (residues 317-363), coordinates two

zinc ions in a ‘cross-braced’ topology, and adopts a fold common to other PHD fingers (designated the ‘core-PHD finger’ hereafter) (2). The N-terminal region (residues 302-316) possesses another C4-type zinc finger (designated the ‘pre-PHD finger’, Fig. S5*A*), which has not been found to be associated with canonical PHD fingers. Only the core-PHD finger made contacts with the N-terminal four residues of histone H3, a region containing ‘modification cassette 1’ of histone H3, R2, T3 and K4 (Fig. S5*B*) (3).

The N-terminal residues of histone H3 peptide adopt an extended conformation and fit into a shallow negatively charged groove on the PHD finger of UHRF1 (Fig. S5*A*). The N-terminal amino group of the histone H3 tail donates direct hydrogen-bonds to the backbone carbonyl oxygen atoms of P353 and E355 in UHRF1 and forms a water-mediated interaction with S354 and D356 (Fig. S5*B*). The side chain of H3-R2 fits into an acidic cavity in the PHD finger, in which the guanidino nitrogen atoms of H3-R2 are strictly recognized through hydrogen bonds with C333, D334 and D337 of UHRF1 (Fig. S5*B*). The aliphatic chain of H3-R2 is stabilized by a hydrophobic interaction with M332. A short segment from R2 to K4 of the histone H3-tail forms intermolecular main chain hydrogen bonds with the β-strand of the PHD finger (residues 330-333) (Fig. S5*B*). The aliphatic chain of the H3-K4 side chain is accommodated in a surface pocket of the PHD finger, and make hydrophobic contacts with the M332 and Q330 side chains of UHRF1. However, no clear electron density was observed for the Nξ atom of H3-K4, indicating that the PHD finger does not recognize H3-K4 (Fig. S5*B*). Consistent with this, methylation of H3-K4 had a small effect on the binding affinity of the histone H3 tail for the PHD finger, as shown by ITC measurement (Table S2 and Fig. S1).

No direct interaction was observed between the PHD finger and R8 and K9 of the histone H3 tail. However, residues Q5-K9 of histone H3 formed hydrogen bonds and hydrophobic interactions with fore residues (E355, Y359, R364 and N365) in the C-terminal region of a neighboring PHD finger molecule in the crystal, allowing the clear electron density corresponding to residues Q5-K9 of histone H3 to be observed.

Structure of TTD-PHD in the asymmetric unit. Four TTD-PHD complexes, designated as complexes A, B, C and D, were encompassed in the crystal asymmetric unit (Fig. S12). Although the electron density of TTD was clearly assigned in all four complexes, that of the PHD finger was unobservable in two complexes (in complexes C and D). Clear electron density in a 2|*Fo*| - |*Fc*| difference Fourier map was observed for the ten N-terminal residues of H3 in complex A and the nine N-terminal H3 residues in complex B (Fig. 3*A*). The hydrogen bonds between N-terminal amino group of the H3 tail and backbone carbonyl oxygens of E355 and D356 of the PHD finger are observed in complex A, but not in complex B. Whereas the four TTDs are tightly packed against one another in the crystal, the PHD fingers in complexes A and B have less contact with the other complexes, and are solvent exposed (Fig. S12*B*-*C*). The B-factors of the PHD moieties are higher than those of the TTDs: the average B-factor of main chain non-hydrogen atoms in the PHD finger (residues 302-364) in complexes A and B is 113.3 $Å^2$, whereas that in the TTDs (residues 134-284) in complexes A-D is 63.1 $Å^2$ (Fig. S12*D*-*F*). The domain junction (residues 299-301) exhibits a higher average B-factor (102.9 $Å^2$) as compared with the linker region (67.8 $Å^2$), suggesting that the domain junction between TTD and the PHD finger also retains flexibility. SAXS data also supported the flexibility between the reader modules in solution because the *P*(*r*) function of wild-type TTD-PHD showed broader distribution to some extent than that calculated from the crystal structure (Fig. S4*C*).

The TTD-PHD structures of complexes A and B are essentially the same, with an r.m.s. deviation of 0.785 Å over 208 Cα atoms. The average B-factors of the PHD finger and the histone H3 peptide in complex B (123.7 $Å^2$ and 94.2 $Å^2$, respectively) are higher than those in complex A (98.8 $Å^2$ and 77.7 $Å^2$, respectively). These differences may be due to non-equivalent crystal packing effects on the PHD fingers. Conformation of the inter-module junction (residues 299-301) are essentially conserved in complexes A and B, and is likely to take part in maintaining the ring shape structure within a certain range of flexibility regardless of the H3 binding. On the bases of the results of structural and biochemical analysis of the linker mutant TTD-$PHD_{R295A/R296A}$ (Figs. 1*C* and 4), the inter-module

junction appears to adopt preferentially the conformation observed in our structure as far as the inter-module linker appropriately interacts with TTD. The structure in the vicinity of the junction implies possible electrostatic and solvent mediated interactions to restrain the relative orientation of PHD to TTD, although any direct interactions are not clearly observed at the current resolution (Fig. S12*G*). However, we cannot completely exclude the possibility that the free form TTD-PHD has different or additional domain interface compared with the H3-bound form. In the main text, the structure of complex A is described.

Possibly due to the high B-factors of the PHD finger region and the lower resolution of the structure of the TTD-PHD:H3 complex (2.9 Å resolution) as compared with the PHD:H3 complex (1.4 Å resolution), a few contacts observed in the PHD:H3 complex could not be identified in the TTD-PHD:H3 complex (see Fig. 2*B* and Fig. S5*B* for comparison). Nevertheless, recognition of cassette 1 in the histone H3 tail by the PHD finger seems to be essentially the same in the PHD:H3 and TTD-PHD:H3 complexes, because most of the contacts observed between the PHD finger and the histone H3 tail in the structure of the TTD-PHD:H3 complex (Fig. 2*B* and S7) are conserved in the PHD: H3 complex (Fig. S5*B*). In addition, the structure of the N-terminal region of histone H3 from A1 to K4 and the PHD finger are nearly the same in these complexes, as shown by the overlay representation (Fig. S6*A*). This structural feature was also supported by the ITC binding data, showing that the modifications on these N-terminal H3 residues caused equivalent negative effects on the H3 binding affinities for the isolated PHD finger and TTD-PHD (Table 1 and Table S2).

Phosphorylation of S298 in *E. coli*. TTD-PHD harboring phosphorylated S298 was prepared as a recombinant protein co-expressed with rat PKA in *E. coli* (1). Phosphorylation of TTD-PHD at S298 was confirmed by a mobility shift assay using Phos-tag SDS-PAGE (Fig. 4*C*). PKA treated TTD-PHD exhibited a significant mobility shift in comparison with the band for non-phosphorylated TTD-PHD, indicating that almost of all the protein was efficiently phosphorylated. The corresponding shift was not observed either for an S298D TTD-PHD mutant or for alkaline

phosphatase treated TTD-PHD$_{S298ph}$ (Fig. 4*C*). Furthermore, linear ion trap ETD MS/MS spectrum identified a triple charged ion (*m*/*z* 580.6) corresponding to the tryptic phosphopeptides S(phos)GPSC(cam)KHC(cam)KDDVNR (residues 298-311) and ART(phos)IIK (residues 208-213) derived from TTD-PHD$_{S298ph}$ (Fig. S10). In the crystal structure of TTD-PHD, the additional phosphorylation site, T210, was located far away from the histone H3 binding site and the inter-module linker binding site. Therefore, the histone H3 binding affinity of TTD-PHD might not be influenced by phosphorylation of T210.

SI Methods

Protein preparation. DNA fragments encoding the PHD finger (299-366), TTD (123-285), TTD-linker (123-300) and TTD-PHD (123-366) of human UHRF1 were each amplified by PCR and cloned into modified a pGEX4T-3 plasmid (GE Healthcare Bio-Sciences) engineered for protein expression with an N-terminal glutathione S-transferase (GST) and small ubiquitin like modifier-1 (SUMO-1) fusion tag, designated the pGEX-ST1 vector. For ITC measurements, the TTD-PHD$_{R295A/R296A}$ mutant was generated by the QuickChange method (Stratagene, LA Jolla, CA). We also prepared TTD-PHD with a deletion of residues 167-175 for crystallography, which was essential for successful crystallization. Deletion of the disordered loop region in TTD did not affect the binding affinity of TTD-PHD for the H3-K9me3 tail (Table S2 and Fig. S3).

Each protein was over-expressed in *E. coli* strain BL21 (DE3). Cells were grown at 37°C in Luria-Bertani (LB) medium and induced with 0.2 mM isopropyl-β-D-thiogalactopyranoside (IPTG) when they reached an optical density of 0.5~0.6 at 660 nm. For the PHD finger, the cells were incubated at 30°C for 3 h; for the other constructs, the cells were incubated at 15°C overnight.

All proteins were purified by following the same protocol as described below but by using a buffer without zinc acetate (ZnOAc) for isolated TTD and the TTD-linker. The cells were harvested, re-suspended in lysis buffer [50 mM Tris-HCl (pH 8.0) containing 300 mM NaCl, 1 mM dithiothreitol (DTT), 30 μM ZnOAc, 10% glycerol and 0.2 mM phenylmethylsulfonyl fluoride (PMSF)] and disrupted by sonication on ice. After centrifugation, the supernatant was applied to a GST affinity column of glutathione Sepharose 4 Fast Flow (GE Healthcare Bio-Sciences) equilibrated with PMSF-free lysis buffer. The GST-SUMO-1 fusion protein was eluted with reduced glutathione and then the SUMO-specific protease GST-SENP2 was added to the solution to remove the GST-SUMO-1 tag. The protein was further purified by anion-exchange chromatography using a HiTrap Q HP column and by size-exclusion chromatography using a HiLoad 26/60 Superdex75 column (GE Healthcare Bio-Science). The protein stored buffer for crystallization is 10 mM Tris-HCl (pH 8.0) buffer containing 100 mM NaCl, 1mM DTT and 50 μM ZnOAc.

Preparation of TDD-PHD$_{S298ph}$ using a *E. coli* phosphorylation system. A cDNA fragment encoding rat cAMP-dependent protein kinase (rPKA, residues 1-350) was amplified by PCR and sub-cloned into a pRSF-1 vector (Novagen) using the *Bam*HI and *Not*I cloning sites. Next, 500 ng of pRSF-1 rPKA vector and 500 ng of pGEX-ST TTD-PHD vector were used to co-transform 50 µl of *E. coli* BL21 (DE3) competent cells. After incubation for 30 min on ice, followed by heat shock, the bacteria were incubated with 300 µl of LB for 3 h at 37°C and were plated on an LB plate containing ampicillin and kanamycin. The cells were grown at 37°C in LB medium or M9 medium containing $^{15}NH_4Cl$ in preparation for NMR until they reached an optical density of 0.52 at 660 nm, and then induced with 0.1 mM IPTG at 30°C for 3 h.

Phosphorylated TTD-PHD was purified as described above. The efficiency of phosphorylation was confirmed by using Phos-tag^{TM} (NARD institute, ltd. Japan) SDS-PAGE containing 100 µM Phos-tag and 100 µM $MnCl_2$ (4). To verify that the high molecular weight band was phosphorylated UHRF1, the protein was treated with rAPid Alkaline Phosphatase (Roche).

Phosphorylation sites were also identified by mass spectrometry analysis. Phosphorylated TTD-PHD was treated with iodoacetamide to alkylate its cysteine residues and was subsequently digested with trypsin (Sigma, Germany). The tryptic peptide mixtures were analyzed by using a nano-LC-ESI-MS/MS instrument (LTQ Orbitrap Velos, ThermoFisher Scientific). MS spectra were recorded, followed by data-dependent electron transfer dissociation MS/MS spectra. Protein identification was performed by MASCOT (Matrix Science) using the latest Swissprot database (*Human*). *Human* UHRF1 was identified with high sequence coverage (23%, 18 peptides hit). Two phosphorylation sites in *Human* UHRF1 were identified at T210 and S298.

X-ray crystallography of the PHD: H3 complex. Screening trials of co-crystallization were performed with a mixture of 1.5 mM PHD finger and unmodified histone H3 peptide (residues 1-10) at a 1:1.5 molar ratio. A crystal of the PHD finger in complex with the histone H3 peptide was

obtained by using a reservoir solution containing 10 mM sodium citrate and 42% PEGMME2000 at 20°C. All crystals were flash-frozen at 100 K in cryoprotectant containing 20% ethylene glycol. The single-wavelength anomalous dispersion (SAD) data set was collected at the absorption peak of the Zn^{2+} ion (λ = 1.28221 Å) on an ADSC Q210 CCD detector in beam line NW-12A at the Photon Factory-AR (PF-AR) in Tsukuba, Japan. Native crystal data were collected at a wavelength of 1.0000 Å on an ADSC Q270 CCD detector in beam line BL-17A at PF. The SAD and native data sets were processed and scaled at 1.8 Å and 1.4 Å resolution, respectively, using the program *HKL2000* (5). Initially, four Zn anomalous sites were identified with the programs *SHELX C* and *SHELX D*, and the initial phases, which allowed us to perform model building, were obtained with *SHELX E* (6). The initial model was refined against diffraction data at 1.8 Å resolution with simulated annealing and energy minimization methods using the program *CNS* (7). After several cycles of refinement with *REFMAC5* (8), the model was well converged at 1.4 Å resolution. The final model contains residues 299-366 residues of the PHD finger, the first nine residues of the histone H3 peptide, 4 Zn^{2+} atoms, 71 water molecules and 4 ethylene glycol molecules. The crystallographic data and data refinement statistics are given in Table S1.

X-ray crystallography of the TTD-PHD:H3-K9me3 complex. Crystallization of TTD-PHD (residues 123-366) in complex with histone H3 tail was not successful. Single crystals were, however, obtained by deleting residues 123-132 in the N-terminal region and residues 167 to 175 in a loop region that, in the structure of the Tudor:H3 complex (PDB; 3db3), is located on the opposite side of the TTD to the histone binding site. The TTD-PHD:H3-K9me3 complex was prepared by adding a 1.5-molar excess of the $H3_{1-12}$-K9me3 peptide to the protein before concentration using an Amicon membrane with a 10,000 cutoff (Millipore). The crystal was obtained by using a 20 mg/ml concentration of the complex at 4°C and the hanging drop vapor diffusion method with a reservoir solution containing 100 mM Bis-Tris propane (pH 6.5), 200 mM sodium citrate and 20% PEG3350. The crystal was directly frozen in liquid nitrogen using cryoprotectant containing 20% ethylene

glycol.

X-ray diffraction data were collected at a wavelength of 1.0000 Å on an ADSC Q315 CCD detector in beam line BL-5A at PF and scaled at 2.9 Å resolution with the program *HKL2000*. The structure was solved by the molecular replacement using the coordinates of TTD (PDB; 3db3) and the PHD finger of UHRF1 as search models. Four complexes were expected to be contained in the crystal asymmetric unit according to the Matthews coefficient (9) (V_M= 2.91 Å^3/Da and V_{sol}=57.7%). The orientations of TTD in the four molecules (designated A, B, C and D) were successfully determined by using the program *PHASER* (10), but not those of the PHD fingers. Electron densities corresponding to the PHD fingers in molecules A and B were, however, unambiguously observed in the $2|F_o|-|F_c|$ difference Fourier map calculated with molecular replacement phases, which allowed us to build the model manually with the program *Coot* (11). Furthermore, the position of each PHD finger was verified on the anomalous difference Fourier map of the Zn atoms calculated using diffraction data collected at λ=1.0 Å. At this stage, $H3_{1-12}$ containing K9me3 was identified in the $|F_o| - |F_c|$ difference Fourier map. After several cycles of refinement by the program *PHENIX* (12) with non-crystallographic symmetry restraints in the four TTD moieties, the model was converged, resulting in a crystallographic *R* value of 24.2% and a free *R* value of 28.6% for all diffraction data up to 2.9 Å resolution.

The final model consists of residues 133-163, 179-325, 328-344 and 347-364 of molecule A; residues 133-162, 180-344 and 348-363 of molecule B; residues 133-162 and 179-302 residues of molecule C; residues 133-161 and 179-301 of molecule D; residues 1-10 and 1-9 of the histone H3 tails bound to molecules A and B, respectively; seven Zn atoms; and four water molecules. The peptide bond between Gly299 and Pro300 in molecules A and B is in the *cis* conformation. The Ramachandran plot of the final model shows good stereochemistry with 81.2% of residues in the most favorable regions, 17.8 % in additionally allowed regions and 1.0% in generously allowed regions, as defined by the program *PROCHECK* (13) at 2.9 Å resolution. The crystallographic data and refinement statistics are given in Table S1. All figures and surface potentials of the protein were

generated with *PyMol* (14). The TTD-PHD:H3 contacts were analyzed with the program *ligplot* (15).

Small-angle X-ray scattering (SAXS). SAXS measurements were performed with a Rigaku NANO-VIEWER system mounted on a Rigaku FR-D X-ray generator operated at 50 kV and 60 mA. The scattering intensities were recorded with a PILATUS 100K detector. A circular averaging of the scattering intensities was then calculated to obtain one-dimensional scattering data $I(q)$ as a function of q ($q = 4\pi\sin\theta/\lambda$, where 2θ is the scattering angle and the X-ray wavelength $\lambda = 1.5418$ Å). Each sample solution (20 μL) was transferred to a quartz-window cell with a 1 mm path length. To correct for interparticle interference, *I(q)* data were collected at two different protein concentrations (8 mg/ml and 4 mg/ml). However, the intensity profile did not indicate a concentration effect; therefore, the correction for the interparticle interference was not applied.

All SAXS data were analyzed with the software package ATSAS 2.4. The radius of gyration R_g was estimated from the Guinier plot (16) of $I(q)$ in a smaller angle region of $qR_g < 1.3$. The distance distribution function $P(r)$ was calculated in the program GNOM (17), where the experimental $I(q)$ data were used in a q-range from 0.018 to 0.213 $Å^{-1}$. The maximum particle dimension D_{max} was estimated from the $P(r)$ function as the distance r for which $P(r) = 0$ (16).

NMR spectroscopy. Wild-type TTD-PHD, TTD-PHD$_{R295A/R296A}$, TTD-PHD$_{S298ph}$, TTD, TTD-linker and PHD finger uniformly labeled with ^{15}N, were each obtained by growing the bacteria in M9 minimal medium containing $^{15}NH_4Cl$ as the sole nitrogen source. For the preparation of ^{2}H- and ^{15}N-labeled, or ^{2}H-, ^{13}C, and ^{15}N-labeled histone H3 tail (residues 1-20) containing a K9me3 analogue, a GST-SUMO-fused histone H3 tail containing K9-to-cysteine mutant was expressed in bacteria grown in M9 medium containing $^{15}NH_4Cl$ and >98%D_2O (Silantes GmbH, Munich) or ^{13}C-Glucose, $^{15}NH_4Cl$ and >98%D_2O.

Each labeled sample of TTD-PHD, TTD-PHD$_{R295A/R296A}$, TTD-PHD$_{S298ph}$, TTD, TTD-linker and PHD finger was dissolved in 10 mM phosphate buffer (pH 7.4) containing 150 mM NaCl, 1 mM DTT, 30 μM ZnOAc and 9% D_2O. ^{1}H-^{15}N SOFAST-HMQC spectra(18) were acquired at 30°C on a

Bruker DRX-700 spectrometer equipped with a TCI cryogenic probe^{TM}.

The backbone ^{1}NH, ^{15}N, $^{13}C_{\alpha}$ and ^{13}CO chemical shifts were assigned by analyzing 500 μM ^{2}H-^{13}C-^{15}N-labeled H3-K9me3 analogue in 200 μl of H_2O/D_2O solution (90%/10%) containing 10 mM phosphate (pH 7.0), 100 mM NaCl, 1 mM DTT, 30 μM ZnOAc and 2 equimolar non-labeled TTD-PHD. The ^{1}H-^{15}N HSQC, HNCO, HNCA and HN(CO)CA spectra were measured with a Bruker Avance 800MHz spectrometer equipped with a TCI cryogenic probe^{TM} at 30°C. Deuterium decoupling pulses were applied where appropriate. Data processing and analysis were done by using the programs NMRPipe (19) and SPARKY 3.1(20). Secondary structure prediction was done with the program TALOS+ (21). The list of chemical shifts is given in Table S3.NMR titration experiments were performed by stepwise addition of the wild-type TTD-PHD, TTD-PHD$_{R295A/R296A}$, TTD-PHD$_{S298ph}$ and a mixture of isolated TTD and PHD finger in up to a two molar excess of 100 μM H3-K9me3 peptide. The ^{15}N and HN chemical shift changes were monitored in ^{1}H-^{15}N SOFAST-HMQC spectra (18), which were analyzed by SPARKY 3.1.

Additional Supplementary references

1. **Sugase K, Landes MA, Wright PE, & Martinez-Yamout M (2008) Overexpression of post-translationally modified peptides in Escherichia coli by co-expression with modifying enzymes. *Protein Expr Purif* 57(2):108-115.**
2. **Adams-Cioaba MA & Min J (2009) Structure and function of histone methylation binding proteins. *Biochem Cell Biol* 87(1):93-105.**
3. **Fischle W, Wang Y, & Allis CD (2003) Binary switches and modification cassettes in histone biology and beyond. *Nature* 425(6957):475-479.**
4. **Kinoshita E, Kinoshita-Kikuta E, & Koike T (2009) Separation and detection of large phosphoproteins using Phos-tag SDS-PAGE. *Nat Protoc* 4(10):1513-1521.**
5. **Minor ZOaW (1997) Processing of X-ray Diffraction Data Collected in Oscillation Mode. *Methods in Enzymology* 276:307-326.**
6. **Sheldrick GM (2008) A short history of SHELX. *Acta Crystallogr A* 64(Pt 1):112-122.**
7. **Brunger AT (2007) Version 1.2 of the Crystallography and NMR system. *Nat Protoc* 2(11):2728-2733.**
8. **Vagin AA, *et al.* (2004) REFMAC5 dictionary: organization of prior chemical knowledge and guidelines for its use. *Acta Crystallogr D Biol Crystallogr* 60(Pt 12 Pt 1):2184-2195.**
9. **Matthews BW (1968) Some crystal forms of bovine chymotrypsinogen B and chymotrypsinogen A. *Journal of molecular biology* 33(2):499-501.**
10. **McCoy AJ, *et al.* (2007) Phaser crystallographic software. *J Appl Crystallogr* 40(Pt 4):658-674.**
11. **Emsley P & Cowtan K (2004) Coot: model-building tools for molecular graphics. *Acta Crystallogr D Biol Crystallogr* 60(Pt 12 Pt 1):2126-2132.**
12. **Adams PD, *et al.* (2002) PHENIX: building new software for automated crystallographic structure determination. *Acta Crystallogr D Biol Crystallogr* 58(Pt 11):1948-1954.**
13. **R. A. Laskowski MWM, D. S. Moss and J. M. Thornton (1993) PROCHECK: a program to check the stereochemical quality of protein structures. *J. Appl. Cryst.* 26:283-291.**
14. **W.L.DeLano (2002) http://www.pymol.org/.**
15. **Wallace AC, Laskowski RA, & Thornton JM (1995) LIGPLOT: a program to generate schematic diagrams of protein-ligand interactions. *Protein Eng* 8(2):127-134.**
16. **Glatter O & Kratky O (1982) Small-Angle X-Ray Scattering. *New York: Academic Press.***
17. **Svergun DI (1993) Determination of the Regularization Parameter in Indirect-Transform Methods Using Perceptual Criteria. . *J. Appl. Cryst.* 25:9.**
18. **Schanda P & Brutscher B (2005) Very fast two-dimensional NMR spectroscopy for real-time investigation of dynamic events in proteins on the time scale of seconds. *J Am Chem Soc* 127(22):8014-8015.**
19. **Delaglio F, *et al.* (1995) NMRPipe: a multidimensional spectral processing system based on UNIX pipes. *Journal of biomolecular NMR* 6(3):277-293.**
20. **Goddard TDaK, D. G., (University of California, San Francisco, SPARKY 3.**
21. **Shen Y, Delaglio F, Cornilescu G, & Bax A (2009) TALOS+: a hybrid method for predicting protein backbone torsion angles from NMR chemical shifts. *Journal of biomolecular NMR* 44(4):213-223.**

22. **D. Svergun, Barberato C, & Koch MHJ (1995) CRYSOL - a Program to Evaluate X-ray Solution Scattering of Biological Macromolecules from Atomic Coordinates.** ***J. Appl. Cryst.*** **28:6.**

Table S1 | Data collection and refinement statistics

	PHD:H3 Zn-SAD	PHD:H3 Native	TTD-PHD:H3K9me3 Native
Data collection			
Space group	*C*2	*C*2	$P4_22_12$
Cell dimensions			
a, *b*, *c* (Å)	68.2, 35.4, 34.1	67.2, 36.1, 34.2	145.0,145.0,125.3
α, β, γ (°)	90.0, 108.8, 90.0	90.0, 110.7, 90.0	90.0, 90.0, 90.0
Resolution (Å)	50.00-1.70 (1.76-1.70) *	50.00-1.40 (1.45-1.40) *	50.00-2.90 (2.95-2.90) *
R_{merge} [*1]	7.8 (34.6) *	4.6 (21.4) *	6.9 (38.0) *
$I / \sigma I$	23.5	23.7	13.9
Completeness (%)	99.0 (93.9) *	92.6 (79.5) *	97.6 (96.7) *
Redundancy	6.9 (4.7) *	3.6 (3.1) *	3.5 (3.4) *
Refinement			
Resolution (Å)		31.97-1.40	40.26-2.90
No. reflections		13,317	29,455
R_{work} / R_{free} [*2]		15.9 / 19.6	24.4 / 28.6
No. atoms			
Protein		531	5960
Ligand (histone H3)		73	170
Ion		4	7
Water		72	4
B-factors			
Protein		13.7	72.2
Ligand (histone H3)		21.7	89.1
Ion		19.7	125.9
Water		26.8	49.8
R.m.s. deviations			
Bond lengths (Å)		0.014	0.009
Bond angles (°)		1.512	1.157

*Values in parentheses are for highest-resolution shell. [*1] $R_{merge} = \Sigma_h \Sigma_i |I(h)_i - \langle I(h) \rangle| / \Sigma_h \Sigma_i I(h)_i$, where $I(h)$ is the intensity of reflection h, Σ_h is the sum of all measured reflections and Σ_i is the sum of i measurements of reflection. [*2] R_{work} and $R_{free} = (\Sigma_{hkl} ||Fo| - |Fc||) / \Sigma_{hkl} |Fo|$, where the free reflections (5% and 10% of the total used in PHD:H3 and TTD-PHD: H3, respectively) were used for R_{free} throughout refinement.

Table S2 | Summary of ITC data

Histone peptide	Protein	K_d (μM)	ΔH (kcal/mol)	N	TΔS (Kcal/mol)
H3-K9me3	PHD	1.47 ± 0.07	-6.36 ± 0.30	1.02 ± 0.04	1.47 ± 0.29
	TTD	1.75 ± 0.19	-8.35 ± 0.06	1.17 ± 0.08	-0.62 ± 0.12
	TTD-PHD	0.37 ± 0.01	-12.10 ± 0.67	1.00 ± 0.05	-3.48 ± 0.67
	R295A/R296A	3.27 ± 0.17[*4]	-8.22 ± 0.05	2.06 ± 0.04	-0.86 ± 0.08
	TTD+PHD	1.99 ± 0.28[*4]	-8.27 ± 0.11	2.16 ± 0.06	-0.62 ± 0.07
	S298ph TTD-PHD	8.99 ± 0.65[*4]	-10.52 ± 0.28	1.49 ± 0.01	-3.76 ± 0.28
	TTD-PHD (crystal)[*3]	0.48 ± 0.09	-12.12 ± 0.69	0.99 ± 0.02	-3.65 ± 0.58
unmodified H3	PHD	1.73 ± 0.09	-6.89 ± 0.07	0.99 ± 0.01	0.84 ± 0.07
	TTD	N/D	→	→	→
	TTD-PHD	1.04 ± 0.20	-6.94 ± 0.57	1.02 ± 0.05	3.73 ± 2.32
H3-R2me2a	PHD	12.70 ± 1.57	-3.22 ± 0.11	0.97 ± 0.02	3.35 ± 0.18
	TTD-PHD	10.29 ± 2.93	-4.41 ± 0.26	0.91 ± 0.04	2.16 ± 0.35
H3-R2me2a-K9me3	TTD	1.98 ± 0.82	-7.41 ± 0.70	1.17 ± 0.05	0.27 ± 0.95
	TTD-PHD	3.43 ± 0.02	-8.05 ± 0.19	1.05 ± 0.02	-2.57 ± 0.79
H3-T3ph-K9me3	PHD	N/D	→	→	→
	TTD	6.66 ± 0.51	-6.51 ± 0.16	1.12 ± 0.01	0.44 ± 0.18
	TTD-PHD	N/D	→	→	→
H3-K9me3-S10ph	PHD	2.69 ± 0.22	-5.90 ± 0.13	0.99 ± 0.01	1.57 ± 0.17
	TTD	5.81 ± 0.89	-7.20 ± 0.42	1.16 ± 0.02	-0.18 ± 0.51
	TTD-PHD	2.50 ± 0.13	-6.14 ± 0.11	1.04 ± 0.05	4.50 ± 0.13
H3-A1ac-K9me3	PHD	N/D	→	→	→
	TTD	1.79 ± 0.61	-8.34 ± 0.58	1.15 ± 0.02	-0.61 ± 0.75
	TTD-PHD	N/D	→	→	→
H3-K4me3	PHD	4.50 ± 0.64	-4.36 ± 0.25	1.02 ± 0.04	2.81 ± 0.28
H3-K4me3-K9me3	TTD	4.87 ± 0.57	-8.37 ± 0.18	1.39 ± 0.08	-1.29 ± 0.25
	TTD-PHD	1.31 ± 0.22	-11.39 ± 0.48	0.95 ± 0.04	-3.49 ± 0.39
H3-K27me3*[1]	TTD	N/D	→	→	→
	TTD-PHD	N/D	→	→	→
unmodified H4*[2]	TTD	N/D	→	→	→
H4-K20me3*[2]	TTD	N/D	→	→	→

*[1]; Residues 16-37 of histone H3 peptide containing tri-methylated K27. *[2]; Methyl lysine analogue (see Methods). *[3]; UHRF1 residues 134-366 with residues 167-175 deleted. *[4]; These apparent dissociation constants calculated on the basis of an assumption of 1:1 stoichiometry are not accurate.

Table S3 | Chemical shift (p.p.m.) table of the ^{1}H-, ^{13}C-, and ^{15}N-labeled histone H3 tail (residues 1-20) containing K9me3.

Residue name	CO	CA	HN	N
Ala 1	173.019	51.546	–	–
Arg 2	175.8	55.636	10.111	122.216
Thr 3	–	58.113	7.682	108.744
Lys 4	–	–	–	–
Gln 5	177.655	–	–	–
Thr 6	176.544	63.256	7.71	110.684
Ala 7	178.615	52.968	8.391	124.91
Arg 8	–	57.78	7.738	117.624
Lys 9me3	175.81	58.205	–	–
Ser 10	174.403	57.643	8.445	121.172
Thr 11	175.287	61.347	8.284	114.684
Gly 12	174.726	45.048	8.758	110.905
Gly 13	173.961	44.892	8.317	108.752
Lys 14	176.063	55.501	8.18	120.606
Ala 15	–	50.165	8.27	126.138
Pro 16	176.861	62.697	–	–
Arg 17	176.235	55.638	8.34	121.096
Lys 18	175.958	55.775	8.232	122.518
Gln 19	174.45	55.239	8.139	121.821
Trp 20	–	58.2	7.685	127.511

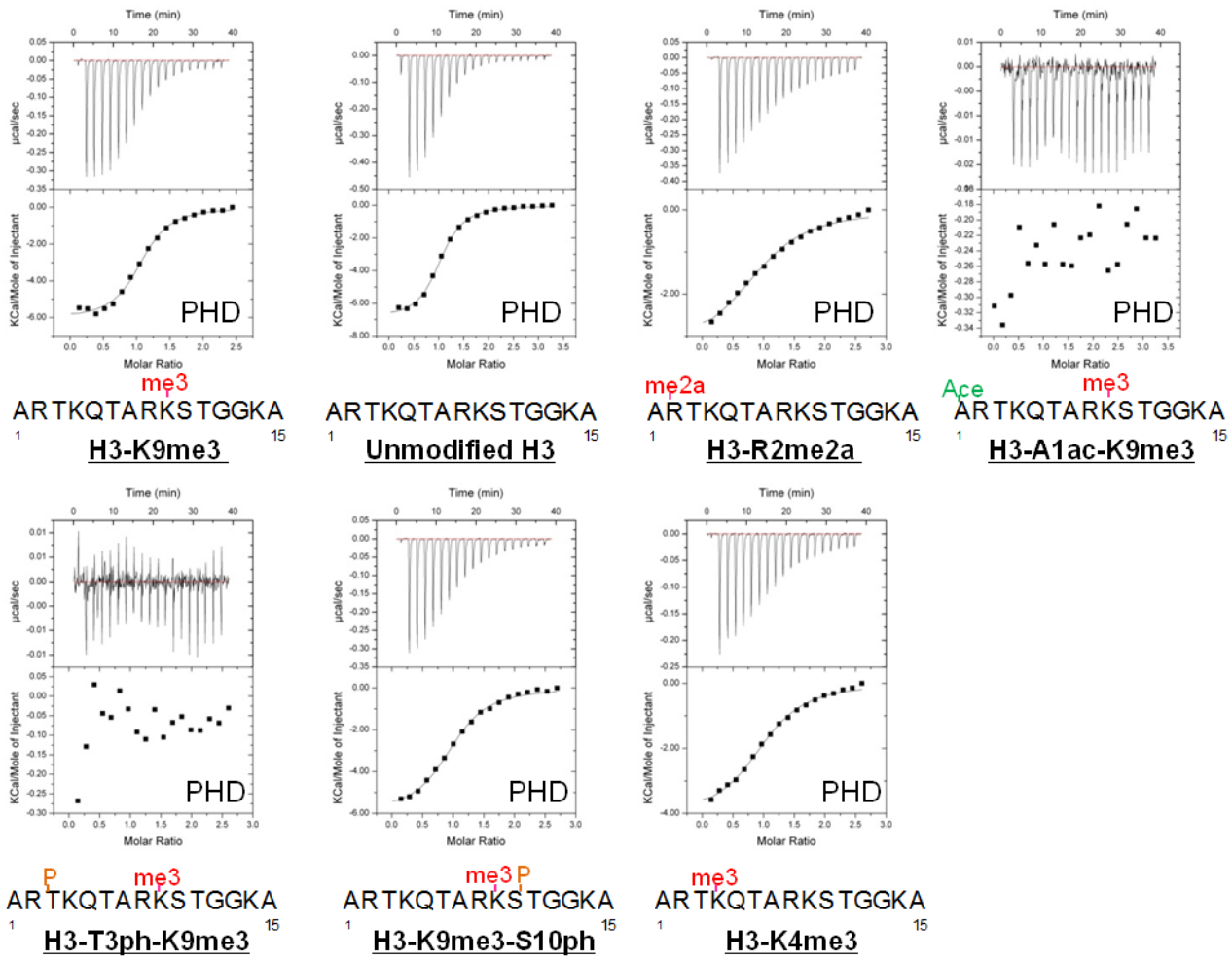

Figure S1. ITC data for titration of the isolated PHD finger with the histone H3 tail containing various modifications. ITC thermograms (upper) and plots of corrected heat values (lower) for binding of the PHD finger to the histone H3 tail are shown. The first data point of each measurement was omitted from the plots in the lower panels and parameter fittings. The K_d, binding enthalpy (ΔH), and stoichiometry (N) values are summarized in Table S2. The histone H3 amino acid sequence including modifications is indicated below the frame. Measurements were performed at 293 K, in a buffer containing 10 mM HEPES (pH 7.4), 150 mM NaCl, 30 μM ZnOAc and 0.1 mM Tris (2-carboxyethyl) phosphine hydrochloride (TCEP).

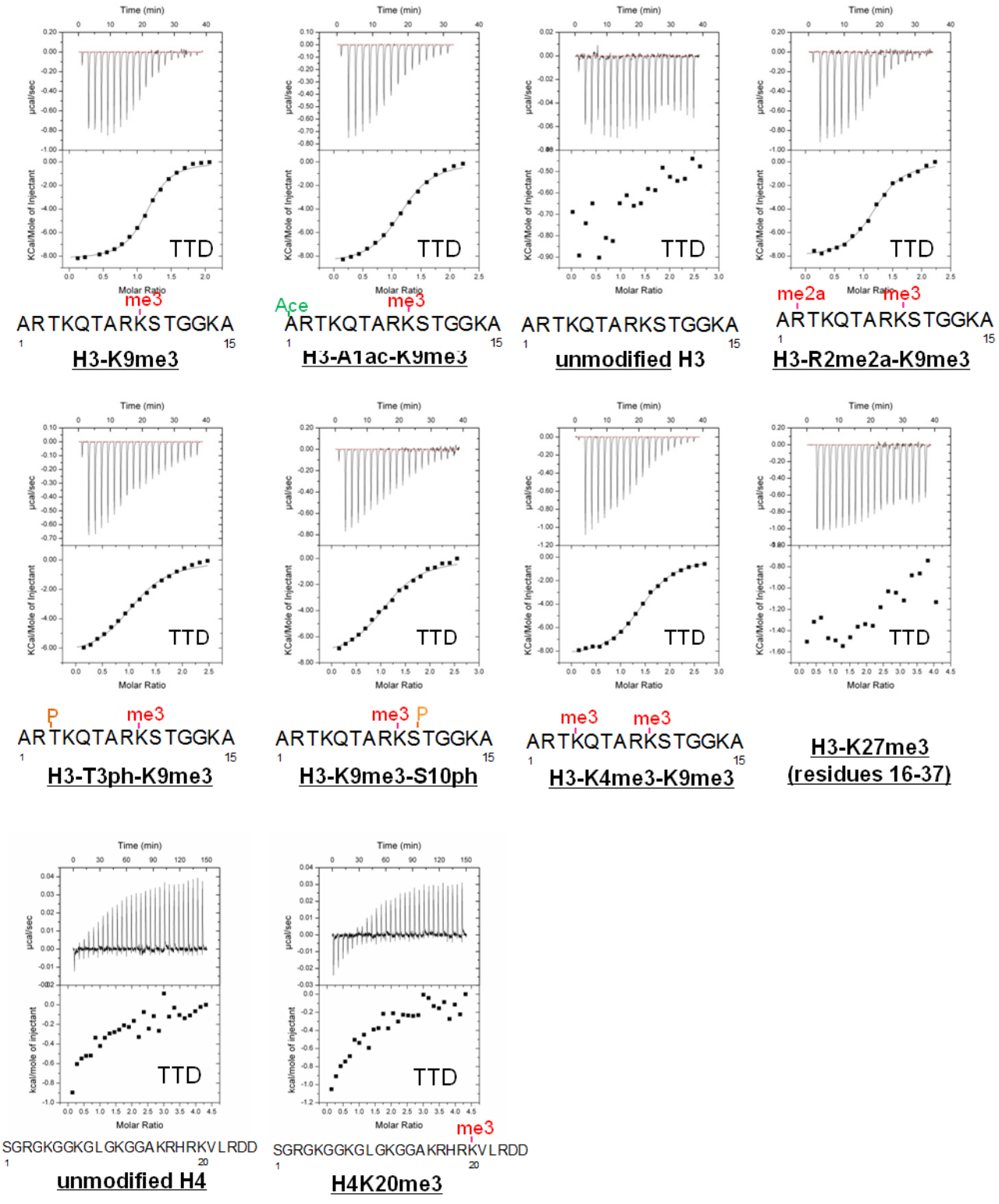

Figure S2. ITC thermograms (upper) and plots of corrected heat values (lower) for binding of isolated TTD to the histone H3 tail. Measurements were performed at 293 K, in a buffer containing 10 mM HEPES (pH 7.4), 150 mM NaCl, 30 µM ZnOAc and 0.1 mM TCEP.

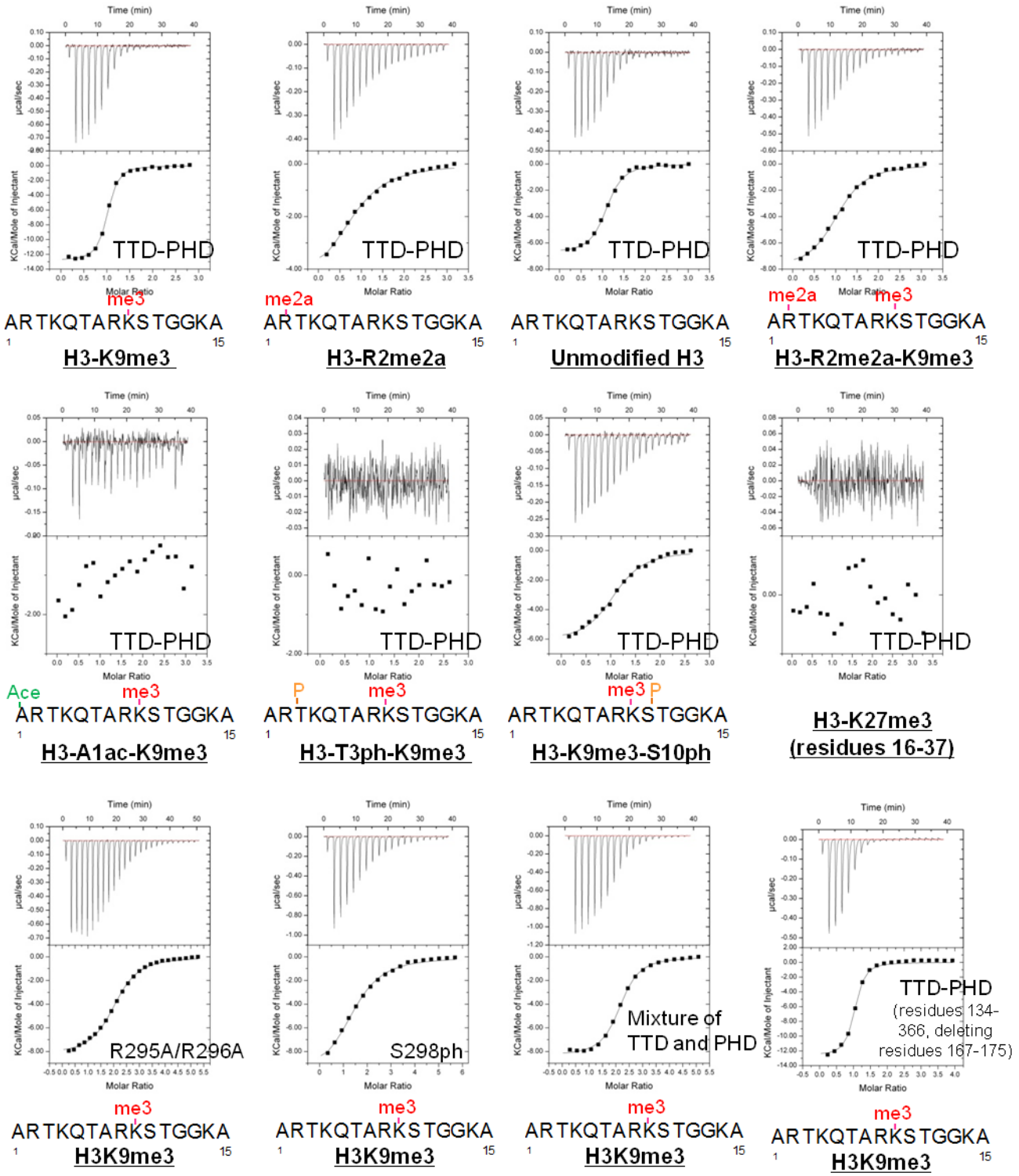

Figure S3. ITC thermograms (upper) and plots of corrected heat values (lower) for binding of TTD-PHD to the histone H3 tail. Measurements were performed at 293 K, in a buffer containing 10 mM HEPES (pH 7.4), 150 mM NaCl, 30 µM ZnOAc and 0.1 mM TCEP.

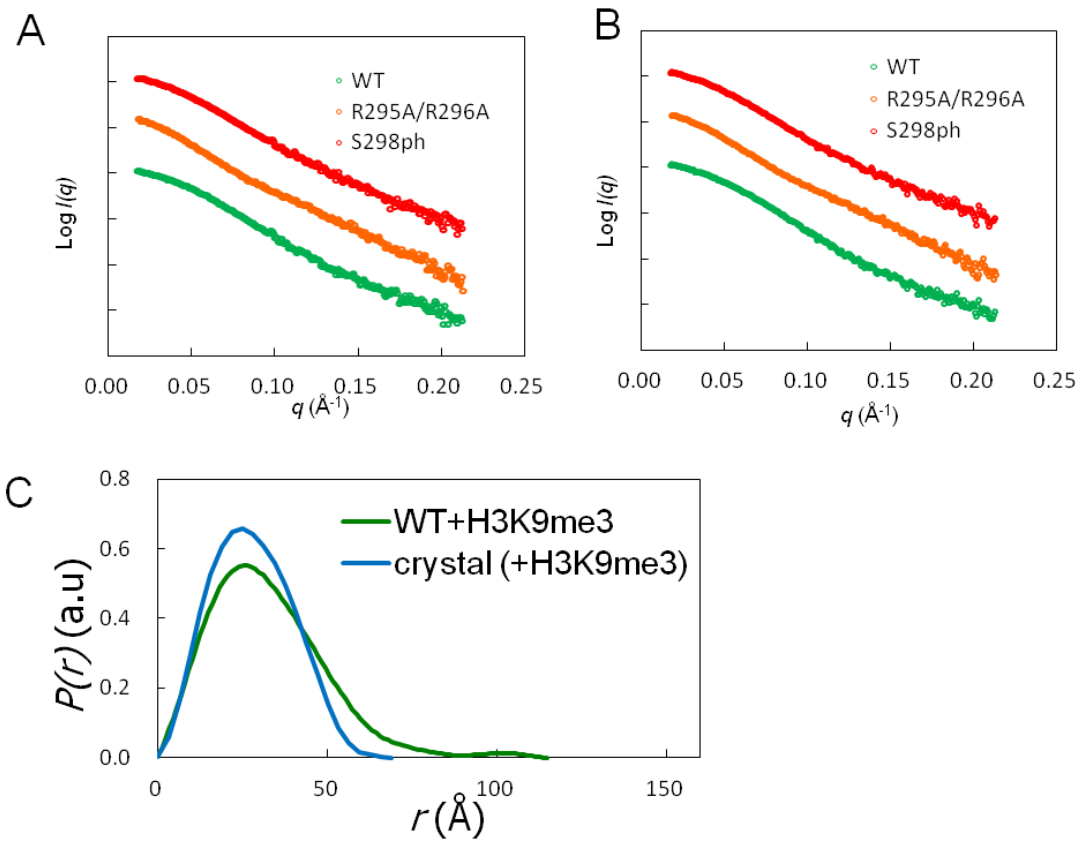

Figure S4. SAXS measurements of experimental *I*(*q*) profiles and *P*(*r*) functions of TTD-PHD.

(A) *I*(*q*) profiles of wild-type (green), R295A/R296A (orange) and S298ph (red) TTD-PHD in the absence of the H3-K9me3 peptide, obtained from SAXS data. The *I*(*q*) scattering curves are appropriately displaced along the axis for better visualization. **(B)** *I*(*q*) profiles of wild-type (green), R295A/R296A (orange) and S298ph (red) TTD-PHD in the presence of the H3-K9me3 peptide. **(C)** *P*(*r*) functions were calculated by the program GNOM. The *P*(*r*) function of the crystal structure was calculated form theoretical *I*(*q*) data generated by the program CRYSOL (22).

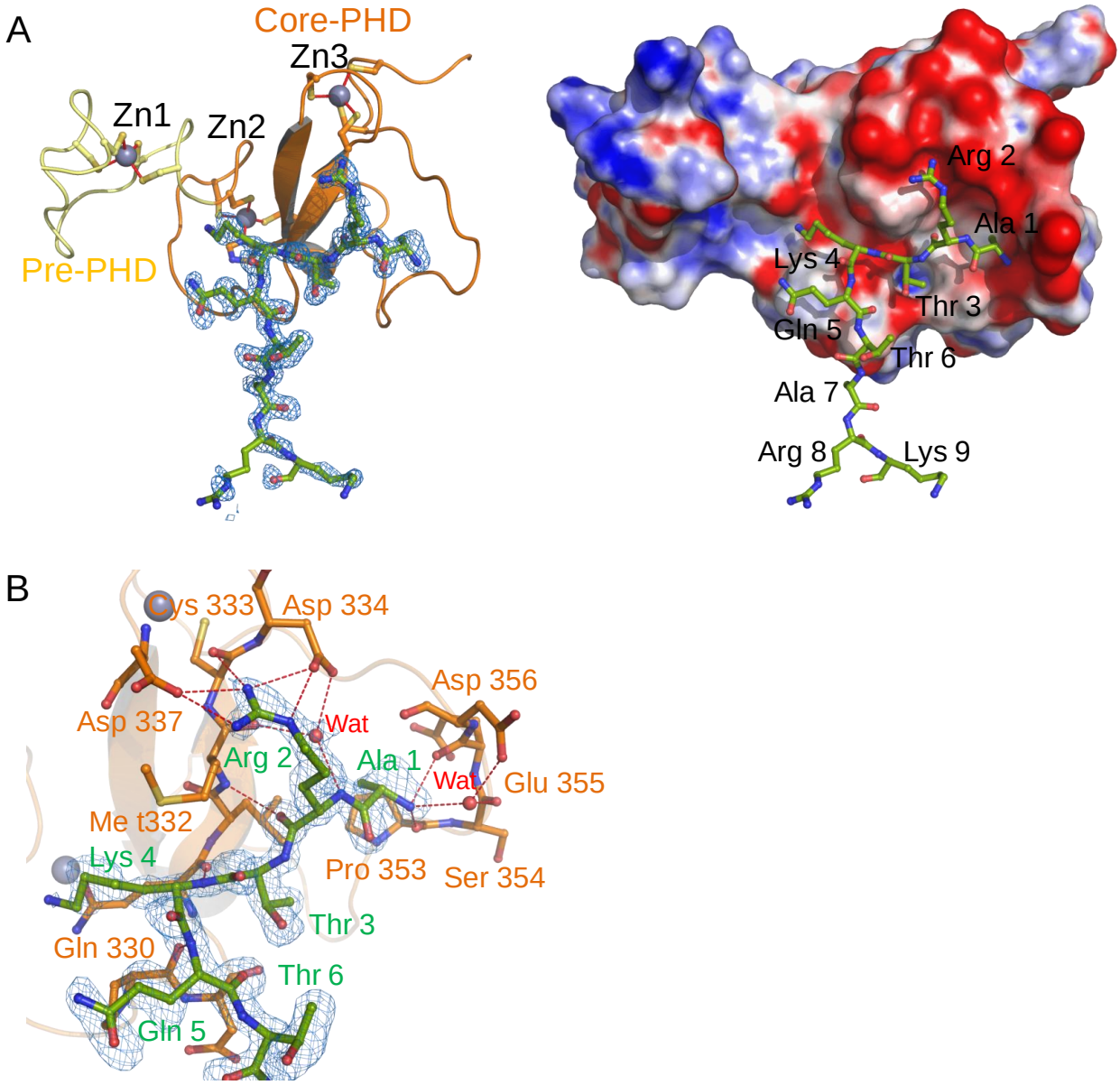

Figure S5. (A) Structure of the isolated PHD finger in complex with the unmodified histone H3 tail. Left panel shows a ribbon diagram of the structure of the PHD:H3 complex. The histone H3 tail is shown as a ball-and-stick model in green. The composite omit electron density map for the histone H3 peptide (>2.0 σ) is shown in blue. The core-PHD and the pre-PHD fingers are shown in orange and light orange, respectively. Zn^{2+} ions are shown as gray spheres. Right panel shows the electrostatic surface potential of the PHD finger in the complex. Surface colors represent the potential from -10 K_BT^{-1} (red) to 10 K_BT^{-1} (blue). **(B) Recognition of the histone H3 tail in the isolated PHD:H3 complex.** Side chains and backbone groups involved in the PHD finger contacts with histone H3 peptide are shown using the same colour code as in Fig. S5*A*. Red dotted lines indicate hydrogen bonds. The composite-omit electron density map for the histone H3 peptide (>2.0 σ) is shown in blue.

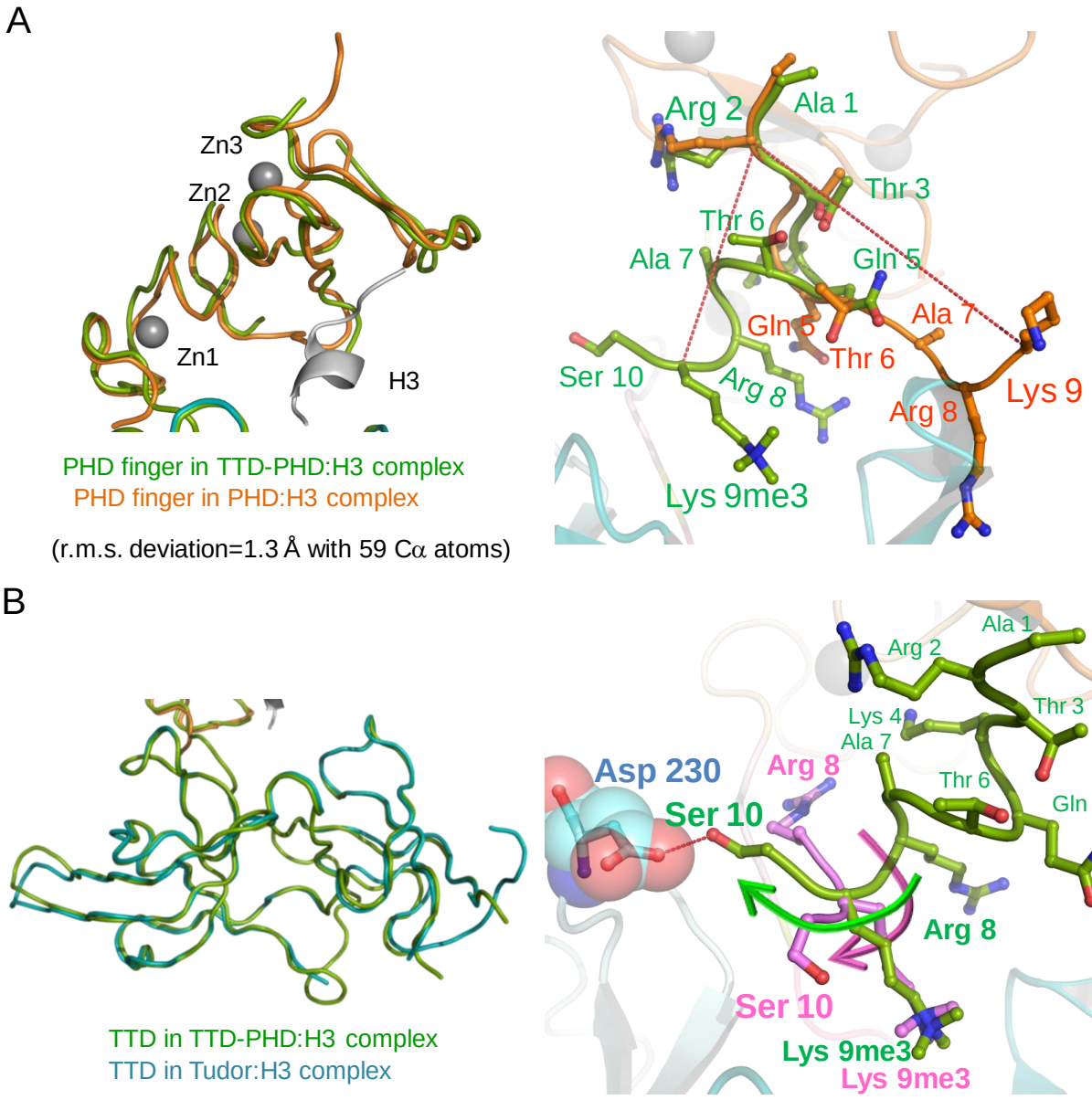

Figure S6. (A) Structure comparison between the isolated PHD finger:H3 complex and the TTD-PHD:H3 complex. Left panel shows the structure of the isolated PHD finger (orange ribbon model) superimposed on the PHD finger in the TTD-PHD:H3 complex (green ribbon model). Zn atoms and the histone H3 peptide are shown as gray spheres and a cartoon model, respectively. Right panel shows an overlay of the histone H3 tail in the TTD-PHD:H3 complex (green) and the isolated PHD:H3 complex (orange). The histone H3 peptide is shown as a ball-and-stick model. Red dotted lines indicate the distances between the Cα atoms of Arg 2 and Lys 9. **(B) Structure comparison between isolated TTD in complex with histone H3 (PDB ID: 3db3) and the TTD-PHD:H3 complex.** Left panel compares the structures of the isolated TTD (blue) and TTD in the TTD-PHD:H3 complex (green). The r.m.s. deviation of the Cα atoms indicates that the structure of the TTD in the TTD-PHD:H3 complex is nearly identical to that in the isolated TTD. Right panel compares the structure of the histone H3 tail in the TTD-PHD:H3 complex (green) and the isolated TTD:H3 complex (pink). Arrows indicate the direction of the backbone segment from Arg 8 to Ser 10 in the TTD-PHD:H3 complex (green) and the TTD:H3 complex (pink), showing that the chain

trace of the histone H3 tail differs between these complexes. As a consequence, Asp 230, shown in a space filling representation, interacts with Ser 10 of histone H3 in the TTD-PHD complex, but not in the TTD:H3 complex.

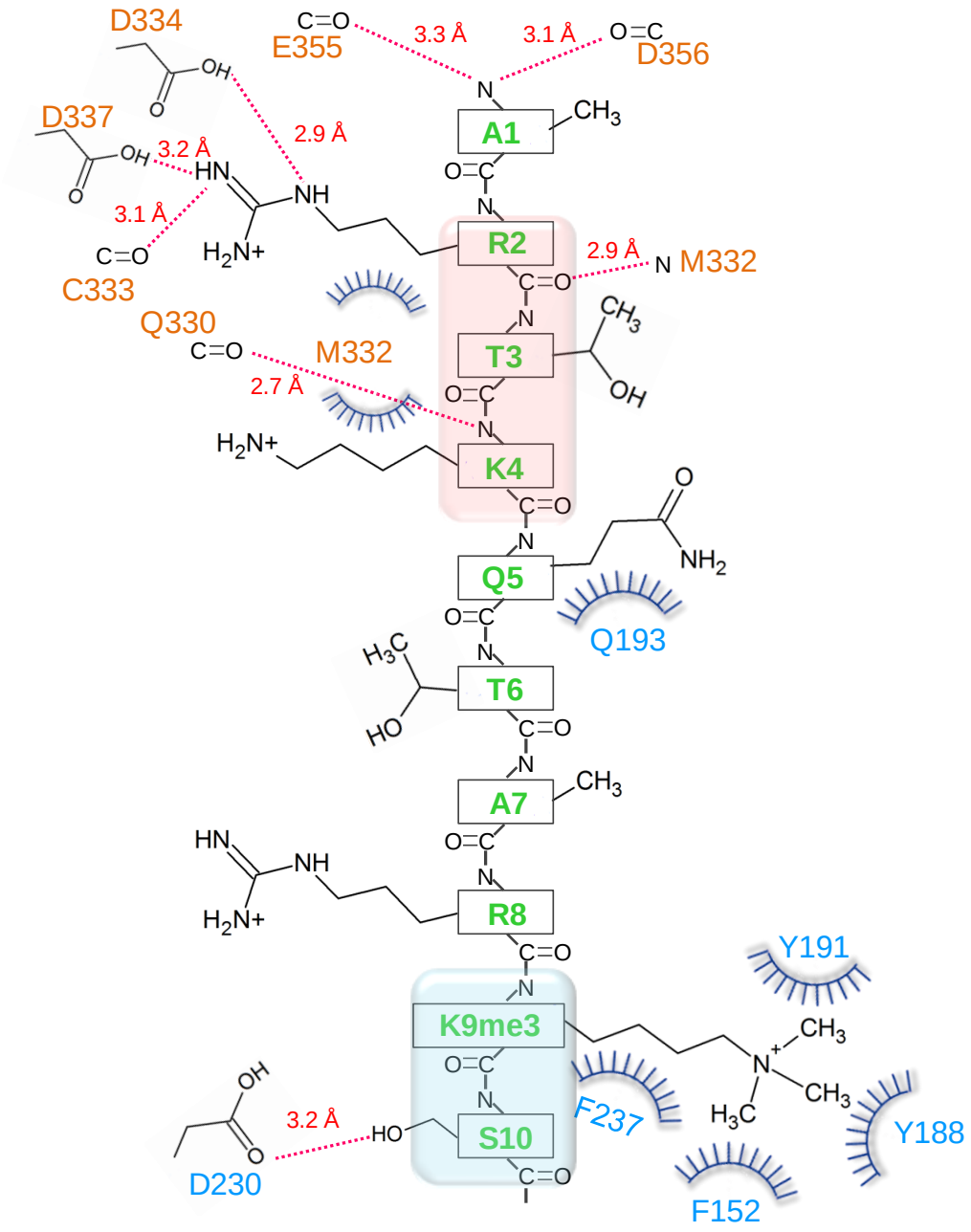

Figure S7. Schematic representation of interactions in the TTD-PHD:H3-K9me3 complex. Red dotted lines and blue half circles indicate hydrogen bonds and hydrophobic interactions, respectively.

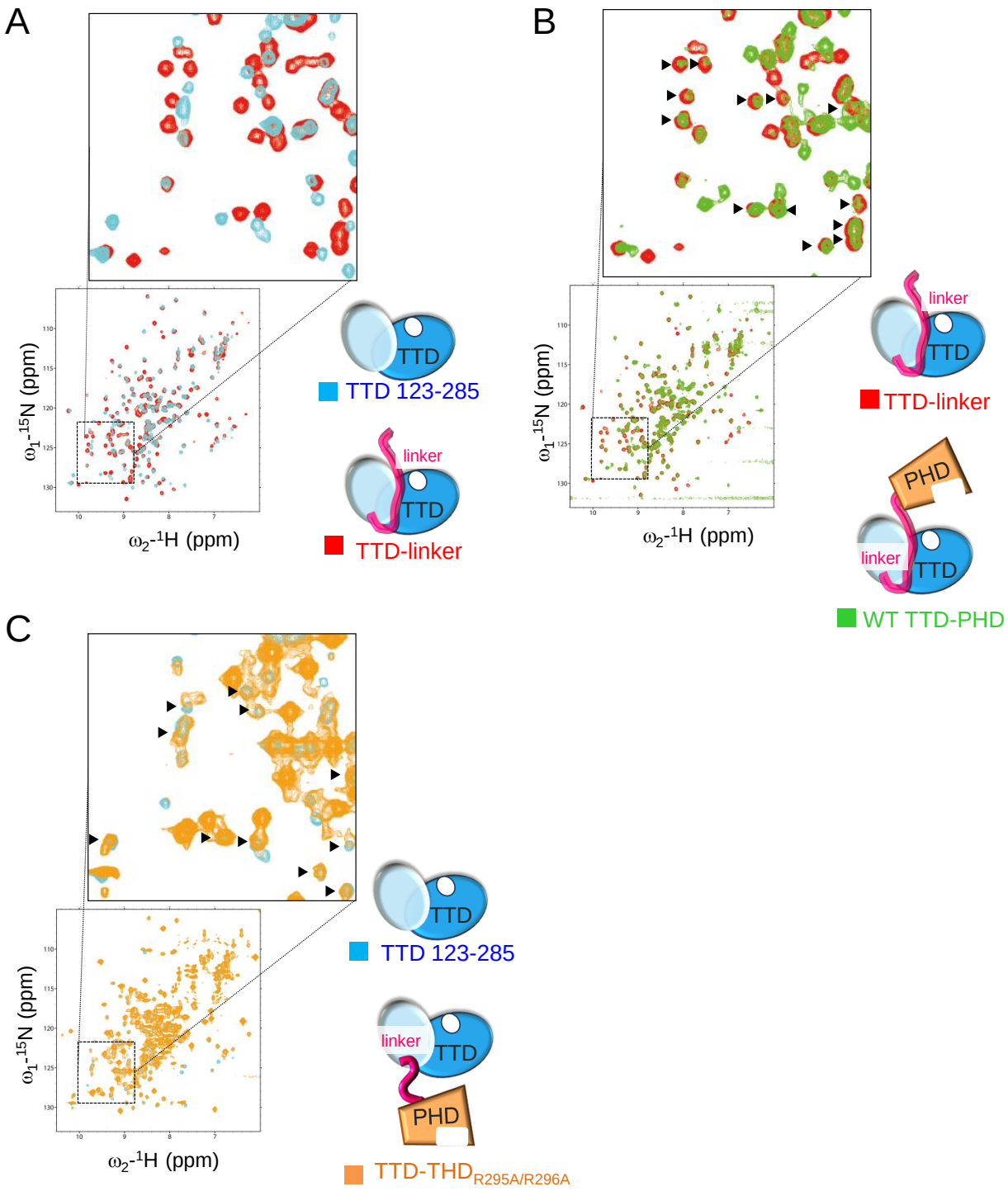

Figure S8. Disruption of the linker:Tudor contacts defined by NMR experiments. Overlay of the ^{1}H-^{15}N correlation spectra of the isolated TTD (123-285) and the TTD-linker (123-300) **(A)**, the TTD-linker and the wild-type TTD-PHD **(B)**, and the isolated TTD and TTD-PHD$_{R295A/R296A}$ **(C)**. Representative cross peaks are indicated by closed triangles. Schematic structures are also represented. Comparison of the ^{1}H-^{15}N correlation spectra between the TTD-linker and TTD alone showed the presence of 65 cross-peaks that are unique to the spectrum of TTD-linker, coupled with the loss of 34 cross-peaks observed in the TTD spectrum (Fig. S8*A*). These 65 peaks that are observed in the spectrum of the TTD-linker but not in that of TTD alone can be attributed mainly to

the 17 linker residues (286-301) and to those located at or near the linker-interacting surface of TTD. Further comparison with the spectrum of TTD-PHD$_{R295A/R296A}$ clearly showed that the linker is detached from TTD in the mutant because most of the signals observed in the spectrum of TTD were present at the same positions in that of the mutant (Fig. S8*C*). These data indicate that the linker was not associated with TTD in TTD-PHD$_{R295A/R296A}$.

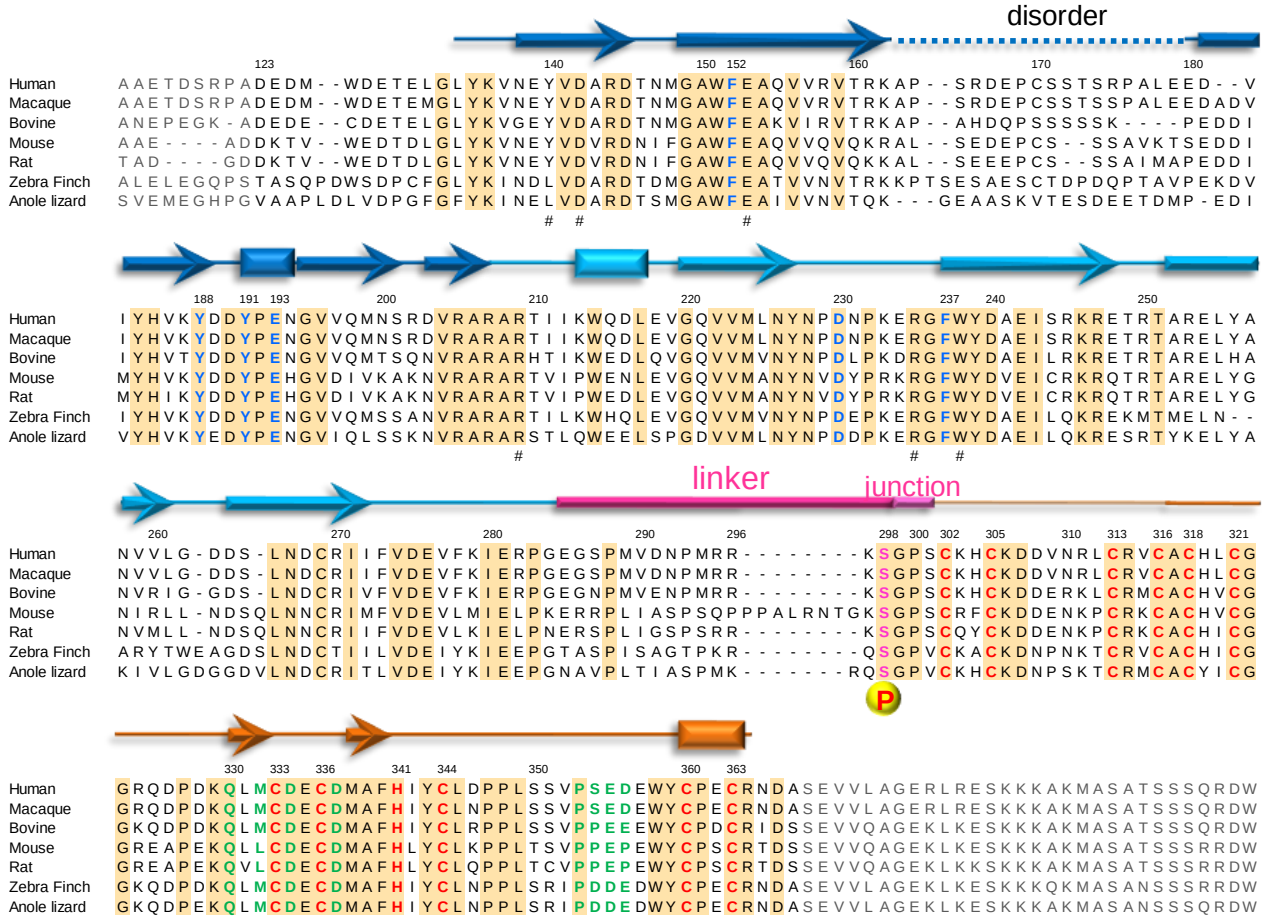

Figure S9. Multiple sequence alignment of the TTD-PHD region in UHRF1 proteins. Numbering is based on the sequence of TTD-PHD of human UHRF1. Secondary structural elements of human TTD-PHD are indicated above the sequences, and disordered regions are indicated by broken lines. Letters in blue, green and red indicate the positions of the TTD-PHD residues involved in recognition of cassette 2 in histone H3, in recognition of cassette 1 in histone H3, and in Zn coordination, respectively. Ser 298, a site of phosphorylation by PKA1, is shown in pink. A hash symbol (#) under the sequence indicates residues in the TTD that are associated with the linker. Fully conserved amino acids are highlighted in orange.

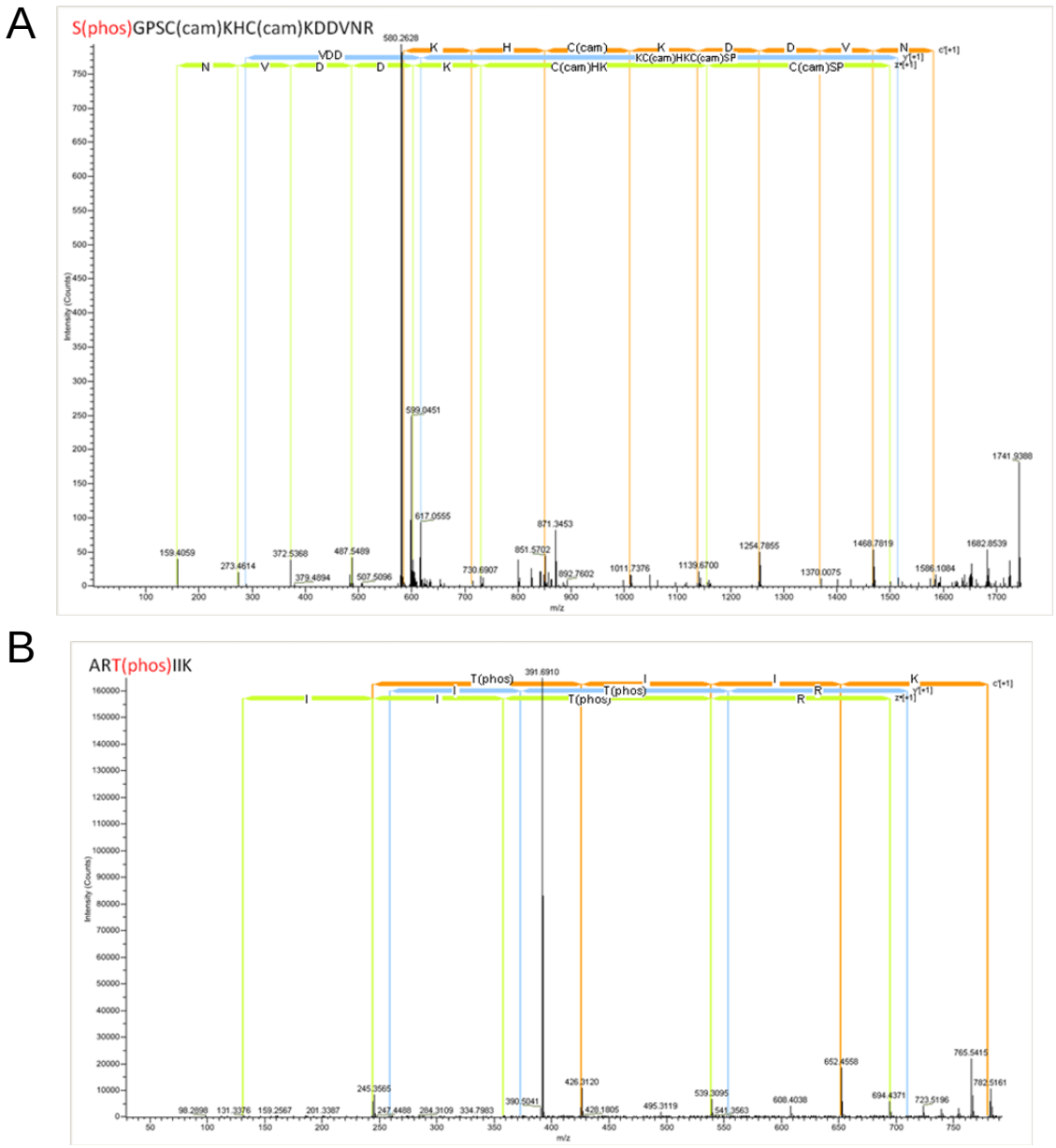

Figure S10. (A) Linear ion trap ETD MS/MS spectrum of a triple charged ion (*m/z* 580.6) corresponding to the tryptic phosphopeptide S(phos)GPSC(cam)KHC(cam)KDDVNR (position: 298-311) from TTD-PHD$_{S298ph}$. The peptide sequence is shown together with the corresponding identified c-/z-type and y-type ions. S(phos) and C(cam) indicate the phosphorylated serine residue and the carbamidomethylated cysteine residue, respectively. Identification of C(cam)SP z-type ion demonstrates phosphorylation of the serine residue at position 298.
(B) Linear ion trap ETD MS/MS spectrum of a triple charged ion (*m/z* 391.2) corresponding to the tryptic phosphopeptide ART(phos)IIK (position: 208-213) from TTD-PHD$_{S298ph}$. The peptide sequence is shown together with the corresponding identified c-/z-type and y-type ions.

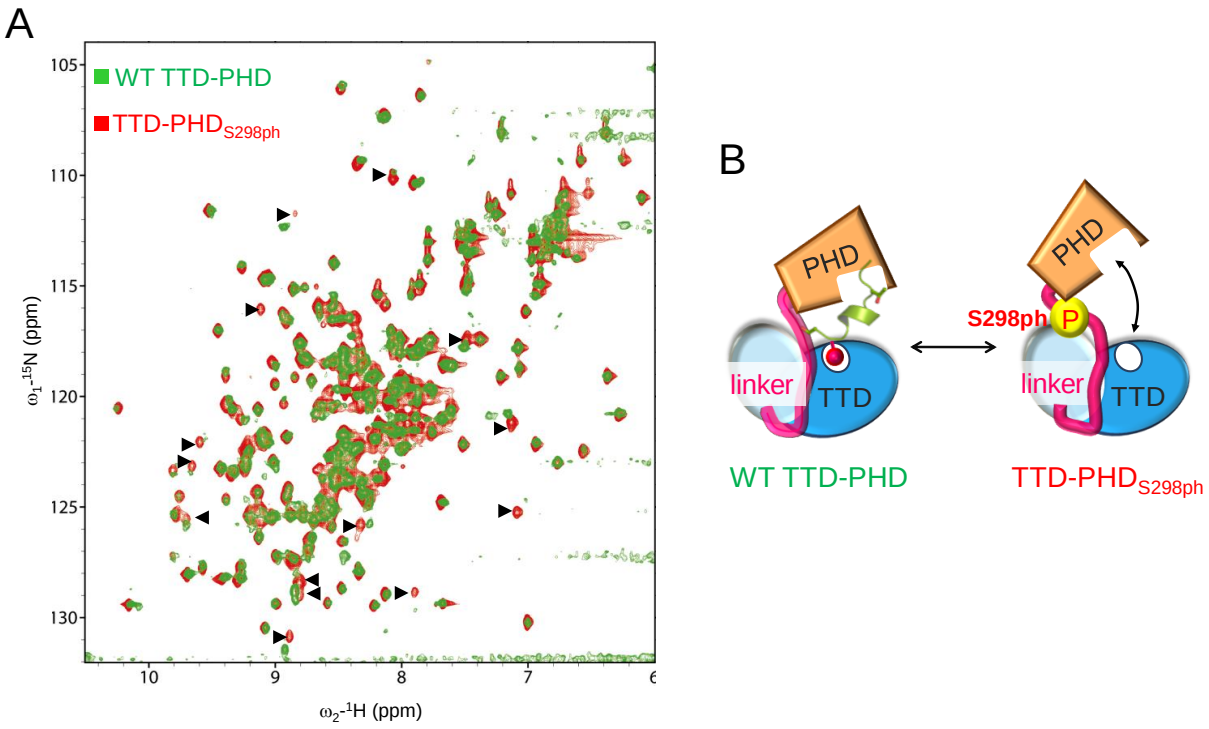

Figure S11. (A) Overlay of the ^{1}H-^{15}N correlation spectra of the wild-type TTD-PHD (green) and TTD-PHD$_{S298ph}$ (red). In the spectrum of TTD-PHD$_{S298ph}$, cross peaks with chemical shift changes caused by phosphorylation are indicated by black triangles. **(B) Schematic representation of wild-type and TTD-PHD$_{S298ph}$.** Local perturbation of the inter-module linker by phosphorylation of S298 caused alteration of the spatial arrangement of the two histone reader modules.

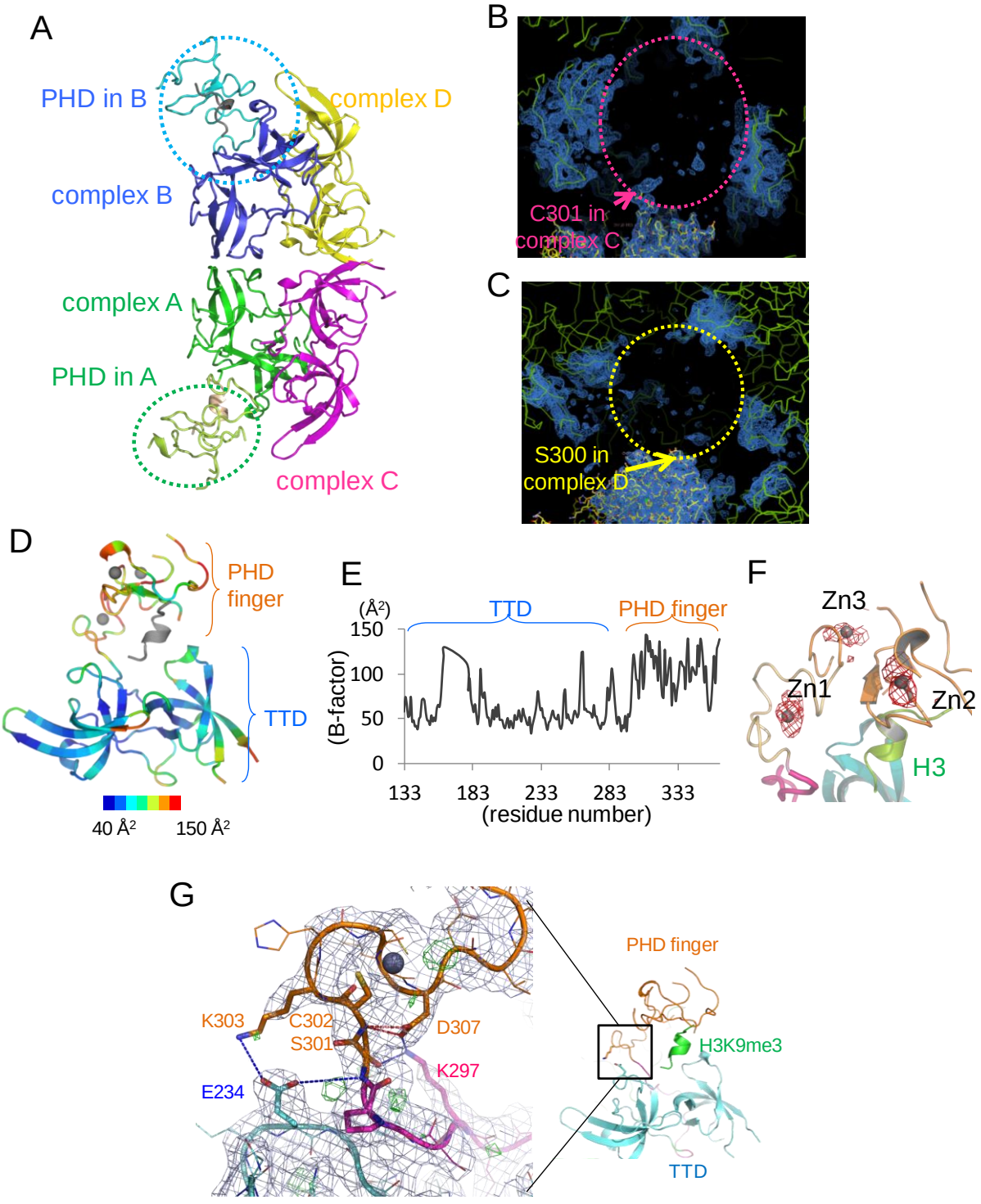

Figure S12. (A) Structure of TTD-PHD in the asymmetric unit. Ribbon diagrams of the four TTD-PHD domains, complexes A, B, C and D, in the asymmetric unit are colored in green, blue, magenta and yellow, respectively. Green and cyan dotted circles indicate the PHD finger moiety in complexes A and B, respectively. **(B), (C) Crystal packing around the region containing the C-terminal TTD and linker in complexes C and D, respectively.** Symmetry related molecules and the 2|*F*o|-|*F*c| difference Fourier map are shown as a green wire model and blue mesh, respectively. Although the electron density of the PHD finger moiety in complexes C and D is invisible, the molecular vacancy may allow for the PHD molecules to exist in the crystal, suggesting that the PHD

moiety retains mobility in these solvent regions. **(D) Ribbon representation of TTD-PHD colored according to the B-factor, as shown in the lower panel. (E) Structure around the Zn^{2+} binding site in the PHD finger.** Anomalous difference Fourier map of Zn^{2+} atoms contoured at 2.0 σ is shown in red with TTD-PHD molecule represented as a cartoon model. **(F) B-factor distribution of TTD-PHD.** The average B-factor (113.3 $Å^2$) of the PHD finger is higher than that of the TTD (63.1 $Å^2$). **(G)** Close up view around the inter-module junction. 2|*F*o|-|*F*c| (blue) and |*F*o|-|*F*c| (green) Fourier map are shown at contoured at 1.0 and 3.0 σ, respectively. The blue dotted lines show the possible electrostatic and polar interactions (4 Å>).